ACS APPLIED POLYMER MATERIALS

pubs.acs.org/acsapm Article

Ionic Liquids as Additives to Improve the Stretchability of Fluorine Rubber/Metal Filler Conductive Elastomers: a Miscibility Study

Wen-Hsien Liu,[⊥] I-Hung Huang,[⊥] Yi-Ting Wu, Dai-Hua Jiang, Wei-Yang Ma, Ying-Chih Liao, and Shih-Huang Tung*

Cite This: *ACS Appl. Polym. Mater.* 2022, 4, 6871−6879 Read Online

ACCESS | Metrics & More | Article Recommendations | Supporting Information

ABSTRACT: We report an intrinsically stretchable conductive elastomer containing fluorine rubber and micrometer-sized silver-coated copper fillers, in which ionic liquids were incorporated to improve the performance. The effects of the miscibility between the ionic liquids and fluorine rubber on the stretchability and conductivity of the composites were particularly focused. The miscibility was analyzed by differential scanning calorimetry (DSC) and small-angle X-ray scattering (SAXS). We compared three different ionic liquids and found that the ionic liquids that are miscible with the rubber can more effectively plasticize the composites to improve the conductivity under stretching, giving a fracture strain more than 400% where the resistance remains below 40 Ω. The effects of the size and shape of the silver-coated copper fillers and the viscosity of the casting solutions were also studied to optimize the performance of the composites. Furthermore, the fluorine rubber was cross-linked to enhance the elastic recoverability of the composites. The cross-linked film shows a fracture strain up to 340% and a good cyclic stretching durability even with the usage of large flakes (15−20 μm) as the conductive fillers.

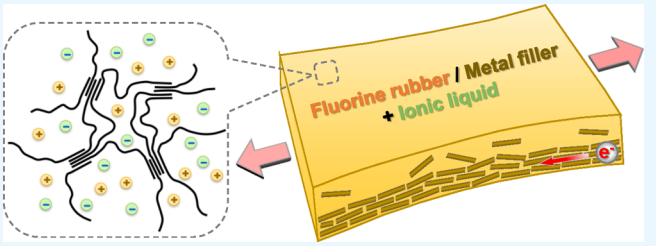

KEYWORDS: *fluorine rubber, ionic liquids, silver-coated copper fillers, miscibility, conductive elastomers*

1. INTRODUCTION

Stretchable conductors are primarily used as electrodes and interconnections that can endure large deformation,[1] potential for various applications, such as electronic skin,[2−4] optoelectronics,[5−7] energy harvesters,[8−10] sensors,[11] and electronic textiles.[12] One promising strategy to prepare intrinsically stretchable conductors is the blending of rubbers and inorganic fillers to form composite conductive elastomers,[13,14] where the low electrical conductivity of rubbers is greatly improved by the conductive fillers, such as carbon nanotubes (CNT),[15−18] carbon black (CB),[19,20] and metal particles or wires.[21,22] To achieve a sufficient high conductivity, the fillers are necessary to contact one another in rubbers. However, a severe aggregation of the fillers leads to a low stretchability of the composites. Thus, the dispersion of the fillers in a rubber matrix is the key factor that determines the electrical and mechanical properties of the composites.[12,15,23] Serval methods have been developed to improve the dispersion of the fillers in rubbers, including surface modifications of fillers[24−27] and incorporation of additives, such as surfactants[12] and ionic liquids (ILs).[28−30]

The interest in ILs has grown dramatically due to their unique characteristics, such as high polarity, nonflammability, high thermal stability, and high ionic conductivity.[31,32] Another important advantage of ILs is their diverse chemical compositions that can impart desired properties, which can be achieved by pairing a variety of organic cations with a wide range of either inorganic or organic anions.[33] ILs have been widely used as additives to enhance the properties of polymers or polymer composites.[34−36] For example, highly stretchable conductors were obtained through the addition of ILs into the originally brittle polymers, such as the poly(3,4-ethylenedioxythiophene):poly(styrenesulfonate) (PEDOT:PSS) complex[37−39] and poly[3-dimethyl-(methacryloyloxyethyl) ammonium propanesulfonate] (PDMAPS).[40] ILs were also used as effective dispersants of fillers to enhance the conductivity and stretchability of the composites. One example is that the agglomeration of CNTs treated with imidazolium-based ILs within poly(vinylidene fluoride) (PVDF) is greatly alleviated due to the cation−π interaction between IL and CNT.[41,42] Another example is that the hybrid conductive fillers of micrometer-sized silver flakes and silver nanoparticle-decorated multiwalled CNTs were mixed with ionic liquids to form highly conductive gels, which could then be well dispersed in PVDF to realize highly conductive stretchable composites.[43] Although numerous studies have reported the efficacy of ILs to improve the

Received: May 11, 2022
Accepted: September 5, 2022
Published: September 12, 2022

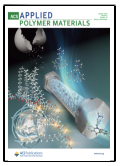

https://doi.org/10.1021/acsapm.2c00801
ACS Appl. Polym. Mater. 2022, 4, 6871−6879

mechanical and electrical properties of composites, most have mainly focused on the specific interactions between fillers and ILs that facilitate filler dispersion in polymers.[44−47] The effect of the miscibility between ILs and polymers is rarely explored.[48]

In this study, we fabricated the free-standing films of stretchable conductive elastomers through the solvent casting method, containing fluorine rubber (F-rubber) as the flexible matrix, micrometer-sized silver-coated copper particles and flakes as the conductive fillers, and ILs as the additives. Silver-coated copper fillers combine the benefits of the low cost of copper and the oxidation resistance of silver that forms a thin protection layer surrounding the readily oxidizable copper.[49−51] ILs with negligible volatility, high ionic conductivity, and strong affinity with metals are suitable for working as plasticizers and dispersants in the rubber/metal filler conductive elastomers. Three ILs were used in this work, and they show high, moderate, and low miscibility with F-rubber, respectively. The effects of several factors on the conductivity and stretchability of the composites were investigated, including the miscibility of the ILs with F-rubber, the size and shape of the silver-coated copper fillers, the viscosity of the solutions used to cast films, and the cross-linking of the rubber. The key finding is that the addition of ILs can effectively plasticize the F-rubber and disperse fillers to improve the conductivity of the elastomers under stretching, especially for the ILs that are miscible with F-rubber.

2. EXPERIMENTAL SECTION

2.1. Materials. F-rubber, poly(vinylidene fluoride-*co*-hexafluoropropylene) (M_n = 123 000 g/mol), was purchased from Daikin Industries, under the trade name of Dai-el G801. Ionic liquids, including 1-ethyl-3-methylimidazolium bis(trifluoromethylsulfonyl)-imide ([EMIM][Tf_2N]), 1-ethyl-3-methyllimidazolium trifluoromethanesulfonate ([EMIM][TfO]), and 1-ethyl-1-methylpyrrolidinium bis(trifluoromethylsulfonyl)imide ([EMPY][Tf_2N]), were purchased from Sigma-Aldrich. The chemical structures of F-rubber and the ILs are shown in Figure 1. The solvent, 4-methyl-2-pentanone (MIBK), was purchased from Honeywell. The cross-linking agents for F-rubber, 1,3(4)-bis[1-(*tert*-butylperoxy)-1-methylethyl]benzene (Luperox F) and 1,3,5-triallyl-1,3,5-triazine-2,4,6(1H,3H,5H)-trione (TAIC), were purchased from Arkema and Sigma-Aldrich, respectively. Silver-coated copper particles and flakes (Ag−Cu) were supplied by Wellion Trade Company, Taiwan. The size, shape, and SEM images of the Ag−Cu fillers are shown in Table S1 of the Supporting Information.

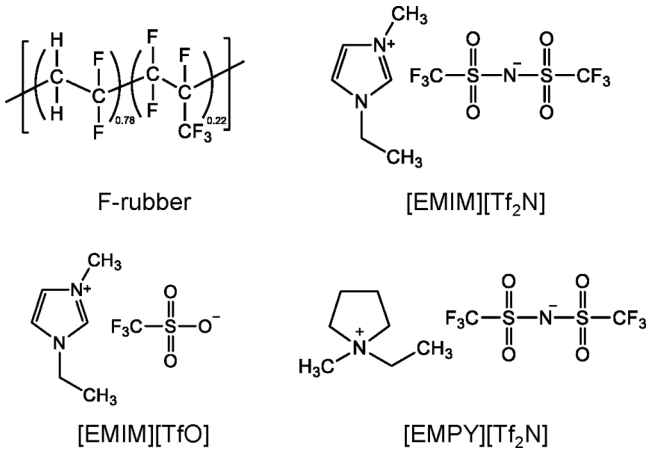

Figure 1. Chemical structures of F-rubber and the ILs used in this work.

2.2. Sample Preparation. To prepare the solutions for film casting, F-rubber, Ag−Cu fillers, and ILs at varying weight ratios as noted in the text were added into MIBK and stirred until uniformly mixed. The weight ratio of F-rubber/MIBK was fixed at 1:3. The solutions were degassed, transferred to glass Petri dishes, and then dried at room temperature for 1 day to remove most MIBK. The films were further dried under a vacuum at room temperature for another day to remove the residual MIBK. The films were ∼0.3 mm in thickness and were peeled from the Petri dishes in a free-standing form for experiments. The optimized cross-linking procedure for F-rubber is as follows. F-rubber and MIBK at a 1:4 weight ratio were mixed, and subsequently, the cross-linking agents Luperox F and TAIC were added to the mixture at a F-rubber/Luperox F/TAIC weight ratio of 1:0.05:0.13. The solutions were then stirred with two-staged heating, 80 °C for 1 h and then 160 °C for 4.5 h, for precuring in the liquid state. The Ag−Cu fillers and ILs were added into the precured solutions and stirred at room temperature for 1 day. The mixtures were degassed, transferred to Petri dishes, and then dried for 1 day. After drying, the films were again treated with two-staged heating, 80 °C for 1 h and then 160 °C for 4.5 h, for curing in the solid state. The free-standing cross-linked films were peeled from the dishes for experiments.

2.3. Characterization. Differential scanning calorimetry (DSC) was measured using a TA Instruments Q20 with a heating/cooling rate of 10 °C/min under a nitrogen atmosphere. Small-angle X-ray scattering (SAXS) was conducted on the beamline BL23A in National Synchrotron Radiation Research Center (NSRRC), Taiwan. The scattering intensity (I) profiles were plotted as functions of wave vector q, where $q = 4\pi \sin(\theta/2)/\lambda$, θ is the scattering angle, and λ is the wavelength of the incident X-ray. The scanning electron microscopy (SEM) images of the cross-sectional structures of films were taken by a JEOL JSM-6700F field-emission SEM at an accelerating voltage of 10 kV. The films were first cut into pieces after quenching in liquid nitrogen. Before imaging, the samples were sputtered with platinum. The element analysis was performed on the energy dispersive spectrometer (EDS) equipped on the SEM instrument. The resistance vs strain curves were measured using a Step-Syn 103H7123-0440 stepping motor (Sanyo Denki, Tokyo, Japan) at a stretching step of 10% strain. The upper limit of the strain for the equipment is 400%. Cyclic stretch-release tests were conducted at 75% strain in a speed of 0.29 mm/s up to 100 cycles. The steady-shear and dynamic rheology were conducted on a TA Instruments AR2000ex stress-controlled rheometer using parallel-plate geometry with a Peltier temperature control at 25 °C. The strain−stress curves were measured on a JSV-H1000 testing machine (JISC, Japan) at a stretching rate of 20 mm/min.

3. RESULTS AND DISCUSSION

3.1. Miscibility between ILs and F-rubber. The miscibility between the ILs and F-rubber was studied using DSC, determined by the change in glass transition temperature (T_g) of F-rubber with the weight ratio of IL to F-rubber, denoted as I_0. The DSC data of the three pure ILs are shown in Figure S1. The T_g's of [EMIM][Tf_2N], [EMIM][TfO], and [EMPY][Tf_2N] are at −85.5, −98.5, and −83.6 °C, respectively. [EMIM][Tf_2N] and [EMIM][TfO] show the melting temperatures (T_m) around −20 °C, both in a liquid state at room temperature, whereas [EMPY][Tf_2N] with a T_m around 88 °C is a crystalline solid at room temperature. The DSC data of the IL/F-rubber blends at I_0 from 0 to 0.5 are shown in Figure S2, and the changes in T_g of F-rubber with I_0 for the three ILs are plotted in Figure 2. The T_g of pure F-rubber is at −17.6 °C. As [EMIM][Tf_2N] is incorporated into F-rubber, T_g decreases with I_0, down to −33.8 °C at I_0 = 0.5. [EMIM][TfO] also lowers the T_g of F-rubber, but not

https://doi.org/10.1021/acsapm.2c00801
ACS Appl. Polym. Mater. 2022, 4, 6871−6879

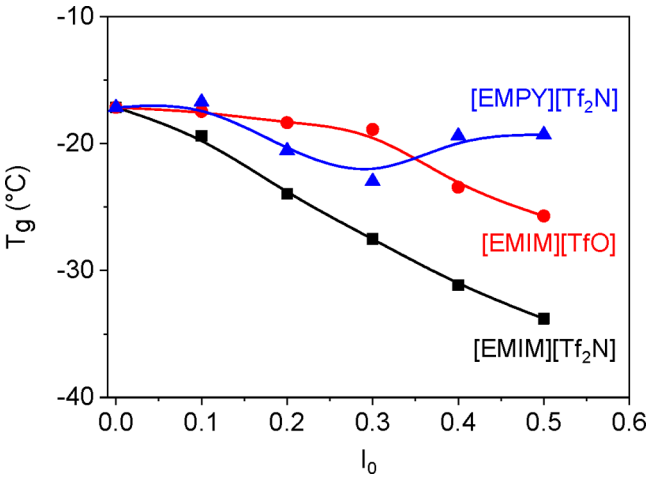

Figure 2. T_g of IL/F-rubber blends as functions of I_0, the weight ratio of IL to F-rubber.

significantly at $I_0 < 0.3$, and the T_g drops to −25.4 °C at I_0 = 0.5. The decay rate of T_g in the [EMPY][Tf_2N] case is in between at $I_0 < 0.3$, and interestingly, T_g increases instead at $I_0 > 0.4$. In Figure S2c, the melting peaks of [EMPY][Tf_2N] can be seen at $I_0 > 0.4$. The increase in T_g can therefore be attributed to the [EMPY][Tf_2N] crystallites formed at a high I_0 that hinder the chain motion of F-rubber. Judging from the DSC data at $I_0 < 0.3$, the miscibility of the ILs with F-rubber is in the order of [EMIM][Tf_2N] > [EMPY][Tf_2N] > [EMIM]-[TfO]. The ILs containing [Tf_2N] anions bearing two trifluoromethyl groups (−CF_3) show a higher miscibility with F-rubber. Compared to [TfO], the size of [Tf_2N] anion is larger, and thus its charge density is lower, which implies a lower electrostatic attraction between [Tf_2N] and the paired cations. Along with the two −CF_3 groups that can interact with F-rubber, the ions of [EMIM][Tf_2N] and [EMPY][Tf_2N] are more likely to dissociate and homogeneously mix in F-rubber.

The structures of F-rubber mixed with the ILs were investigated by SAXS, and the data are shown in Figure 3. F-rubber is a copolymer composed of multiple blocks that tend to assemble into hard and soft domains.[52,53] The hard domains are packed by the regular poly(vinylidene fluoride) blocks, and the soft domains are formed by the random copolymer segments of vinylidene fluoride with hexafluoropropylene.[53] The SAXS profile of pure F-rubber ($I_0 = 0$) is featureless, with an intensity monotonically decreasing with q, indicating that the contrast of the electron density between the soft and hard domains is insufficient to produce the characteristic X-ray scattering. As [EMIM][Tf_2N] is incorporated, the SAXS data for all of the I_0's are essentially the same as that of pure F-rubber (Figure 3a), which implies that [EMIM][Tf_2N] is uniformly dissolved in F-rubber and the contrast of the electron density in the blends remains unchanged, as illustrated in Figure 4a. This is consistent with the DSC thermograms that reveal a highly miscible nature of [EMIM][Tf_2N] with F-rubber. For the [EMIM][TfO] cases, the low-q slopes of the SAXS profiles at $I_0 \geq 0.2$ become steeper than that of pure F-rubber, as shown in Figure 3b. Such a slope change generally suggests a larger structure formed in the samples, presumably the F-rubber-rich and IL-rich domains (Figure 4b) caused by phase separation due to the low miscibility between [EMIM]-[TfO] and F-rubber.

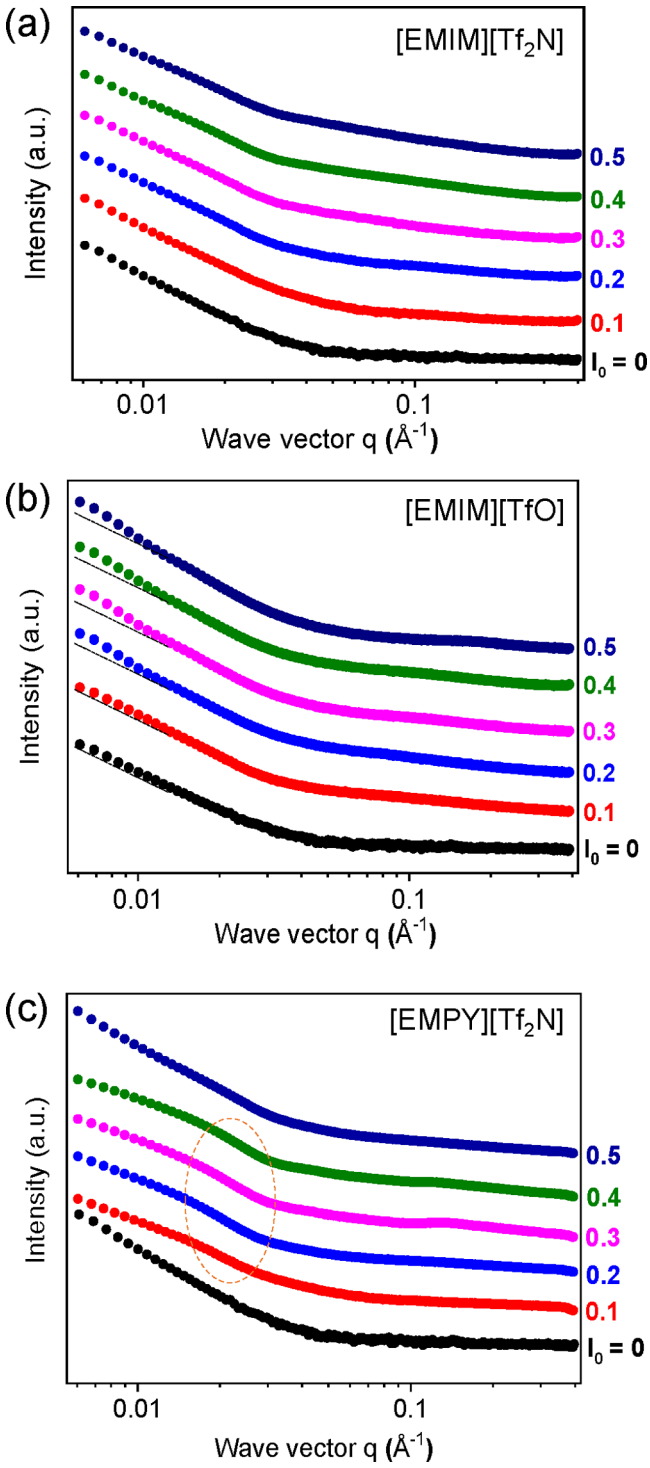

Figure 3. SAXS profiles of F-rubber blended with the ILs at varying I_0: (a) [EMIM][Tf_2N], (b) [EMIM][TfO], and (c) [EMPY][Tf_2N].

Instead of the monotonic changes, the SAXS profiles of the [EMPY][Tf_2N]/F-rubber blends show humps in the q range between 0.02 and 0.03 $Å^{-1}$ (Figure 3c), corresponding to a domain size ∼20−30 nm. A plausible explanation for this scattering characteristic is that [EMPY][Tf_2N] is selectively dissolved in the soft domains where the random copolymer segments are arranged in a disordered manner while the hard domains are nearly intact due to the closer packing of the regular poly(vinylidene fluoride) blocks (Figure 4c). This is

https://doi.org/10.1021/acsapm.2c00801
ACS Appl. Polym. Mater. 2022, 4, 6871−6879

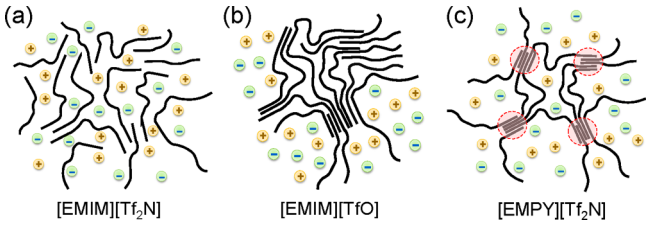

Figure 4. Schematics of the distributions of the ILs in F-rubber: (a) [EMIM][Tf_2N], (b) [EMIM][TfO], and (c) [EMPY][Tf_2N].

supported by the DSC data that show a moderate miscibility of [EMPY][Tf_2N] in F-rubber. Such a distribution of the IL alters the electron density of the soft domains and causes a contrast sufficient to reveal the scattering feature of the hard domains as the humps.[54,55] At I_0 = 0.5, the slope at low q significantly increases, which results from the crystallization-induced phase separation that leads to large pure crystal domains of [EMPY][Tf_2N], in agreement with the DSC data.

The appearance of the films shown in the photographs of Figure S3 confirms the DSC and SAXS results. The [EMIM][Tf_2N]/F-rubber film remains transparent at I_0 = 0.5, indicating that the IL and F-rubber are homogeneously mixed even at high I_0. By contrast, the [EMIM][TfO]/F-rubber film is slightly hazy at an I_0 as low as 0.1 and becomes cloudier as I_0 increases, evidencing the occurrence of phase separation that causes strong light scattering. [EMPY][Tf_2N] shows moderate miscibility with F-rubber, mainly dissolved in the soft domains, and tends to form crystalline aggregates that scatter light at high I_0. This explains why the [EMPY][Tf_2N]/F-rubber films are transparent at I_0 < 0.3 and become cloudy at I_0 > 0.4. The stress−strain curves of F-rubber and its blends with the ILs at I_0 = 0.2 are compared in Figure S4, and the mechanical properties are listed in Table S2. The well-mixed [EMIM][Tf_2N] can effectively soften F-rubber and causes the lowest modulus and tensile strength. [EMIM][TfO] that is phase-separated from F-rubber and [EMPY][Tf_2N] that is selectively dissolved in the soft domains are less effective in softening and thus give rise to higher moduli and tensile strengths at the same I_0. This provides other evidence supporting the distributions of the ILs in F-rubber deduced from the SAXS data.

3.2. Effects of Shape and Size of Ag−Cu Fillers. The effects of the Ag−Cu fillers with different shapes, including spherical particles and flakes, and different sizes on the stretchability and conductivity of the composites were examined. Here, the highly miscible [EMIM][Tf_2N] was adopted for the tests, and the weight ratio of F-rubber/Ag−Cu/[EMIM][Tf_2N] was fixed at 1:3:0.5. The resistance R vs strain curves for the fillers are shown in Figure 5. Overall, the stretchability drastically decreases with increasing size for both spheres and flakes. The composites with a filler size smaller than 5 μm can endure strains higher than 350%, and those with a size larger than 5 μm break at strains below 100%, among which the fracture strain caused by the 15−20 μm flakes is only 20%. The variation in stretchability correlates with the voids formed in the composites during solvent casting, as shown in the SEM images of Figure S5. For smaller spheres, only small holes occur in the composites and the rubber form continuous phase that can withstand a high strain, while for larger flakes, the rubber is unable to fill the space between flakes, thus leaving large voids that cause a low stretchability. In contrast to the stretchability, the fillers with larger size show a higher

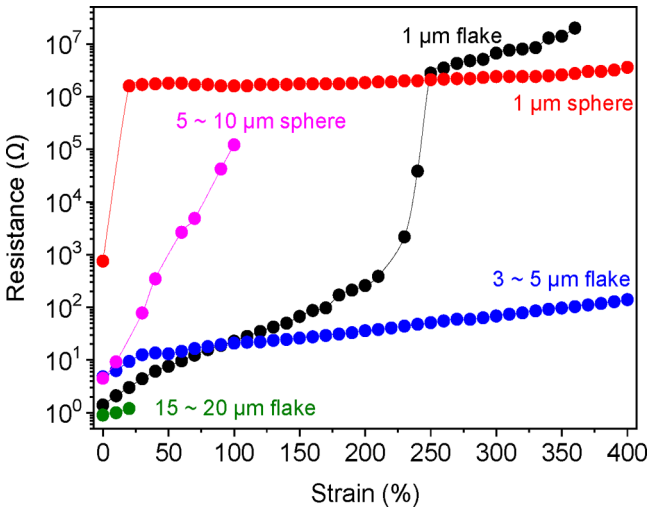

Figure 5. Resistance vs strain curves for Ag−Cu fillers with varying shapes and sizes. The weight ratio of F-rubber/Ag−Cu/[EMIM][Tf_2N] was fixed at 1:3:0.5.

conductivity and the flakes outperform the spheres. This is because larger flakes with high aspect ratios are more capable of forming percolated networks for electrons to transport. The resistance of the composite with 15−20 μm flakes is about 1 Ω before fracturing. Among the fillers, the 3−5 μm flakes show a balanced performance of stretchability and conductivity, with a fracture strain above 400% where the resistance remains below 140 Ω.

3.3. Effects of ILs on Stretchability. The 3−5 μm Ag−Cu flakes were used as conductive fillers to investigate the effects of different ILs on the mechanical and electrical properties of the composites. The weight ratio of Ag−Cu flakes to F-rubber was fixed at 3, and I_0 varied from 0 to 0.5. Figure 6 shows the resistance R as a function of strain for the three ILs, and the normalized resistance with respect to the initial value (R/R_0) is shown in Figure S6. The fracture strain of the composite without ILs is only 20%. For [EMIM][Tf_2N] that is highly miscible with F-rubber, the fracture strain greatly increases with increasing I_0 and exceeds 400% at I_0 = 0.4 and 0.5, between which the composite at I_0 = 0.4 exhibits a lower resistance variation with strain. By contrast, the fracture strains of the composites with [EMIM][TfO] that show a low miscibility with F-rubber are rather low for all I_0's. The highest one is 140% at I_0 = 0.1, and the fracture strains fall to 20% at I_0 > 0.3, a similar level to that without IL. In the case of [EMPY][Tf_2N] that is moderately miscible and crystallizable at room temperature, the fracture strain drastically increases with increasing I_0 until 0.3, and then decreases as I_0 further increases. The composite at I_0 = 0.2 shows the best performance with a fracture strain more than 400% and a resistance below 40 Ω.

The above results manifest that the miscibility between ILs and F-rubber is crucial to the mechanical and electrical properties of the composite elastomers. [EMIM][Tf_2N] is highly miscible in the rubber and can homogeneously mix with the rubber to facilitate the motion of polymer chains and Ag−Cu flakes, which results in a good stretchability as I_0 increases. The conductivity decreases with I_0 due to the dilution of the flakes, and the composite reaches a balanced performance at I_0 = 0.4. When F-rubber is blended with [EMIM][TfO], the mixture phase-separates into IL-rich phases and F-rubber-rich

https://doi.org/10.1021/acsapm.2c00801
ACS Appl. Polym. Mater. 2022, 4, 6871−6879

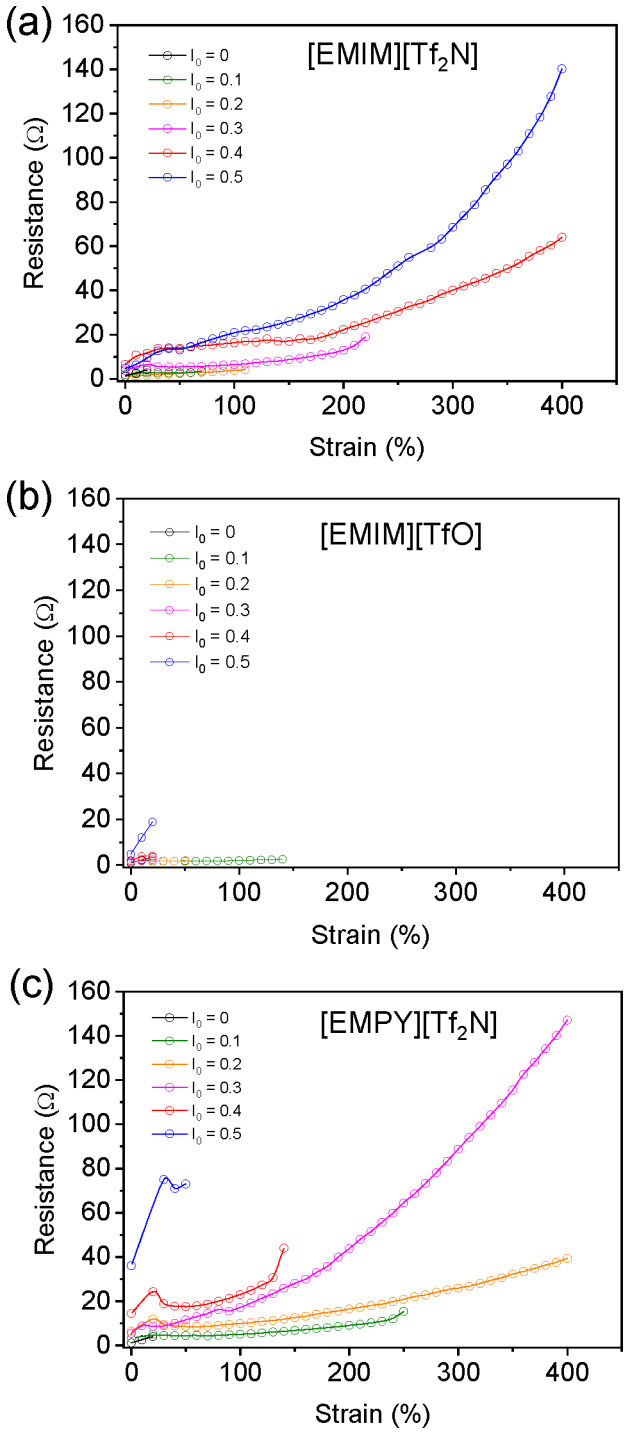

Figure 6. Resistance vs strain curves of the composites with the ILs at varying I_0: (a) [EMIM][Tf_2N], (b) [EMIM][TfO], and (c) [EMPY][Tf_2N]. The 3−5 μm Ag−Cu flakes were used, and the weight ratio of F-rubber/Ag−Cu was fixed at 1:3.

phases because of their low miscibility. The presence of the mechanically weak IL-rich phases should be responsible for the low fracture strains of the composites. For [EMPY][Tf_2N] at low I_0, ∼0.2, the IL dissolves in the soft domains of F-rubber where it is in an amorphous and mobile state and can work as an effective plasticizer. Along with the intact hard domains that maintain the mechanical strength (Figure 4c), the composite thus exhibits superior performance. At I_0 > 0.3, however, the tendency of [EMPY][Tf_2N] to closely pack results in the crystallization-induced phase separation that forms the pure, rigid IL crystals in the composites, which in turn makes a negative impact on the stretchability and conductivity.

3.4. Effects of Solution Viscosity. Because the sizes of the Ag−Cu fillers are on the micrometer scale, such large particles inevitably settle from the solutions due to gravity during the casting process. The sedimentation velocity correlates to the distribution of the fillers in the composite films after solvent evaporation, which can significantly affect the properties of the composites. The major factor that affects the sedimentation velocity is the viscosity of the solutions. Here, the viscosity was controlled by the solvent (MIBK) fraction, and its effect on the performance of the conductive elastomers was investigated. The solutions with a varying MIBK/F-rubber weight ratio (S_0) at a fixed weight ratio of F-rubber/Ag−Cu/[EMIM][Tf_2N] = 1:3:0.5 were prepared. The size of the flakes used in this test is ∼1 μm. The viscosities of the solutions at S_0 = 2, 3, and 4 are 7, 1.5, and 0.3 Pa s, respectively (Figure S7), decreasing with increasing S_0 due to the dilution effect. Figure 7 shows the resistance vs strain

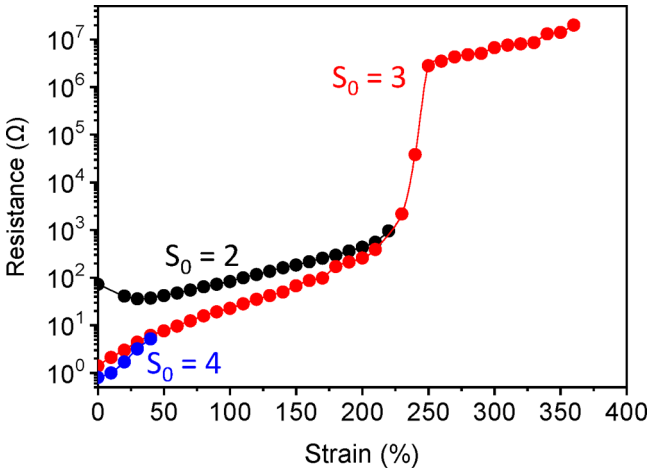

Figure 7. Resistance vs strain curves of the composites cast from the solutions at different MIBK/F-rubber weight ratios S_0. The ∼1 μm Ag−Cu flakes were used, and the weight ratio of F-rubber/Ag−Cu/[EMIM][Tf_2N] was fixed at 1:3:0.5.

curves of the composites cast from the solutions at different S_0. The best stretchability of the composite occurs at S_0 = 3, with a fracture strain of 350%, much higher than the others. Although the resistance decreases with S_0 and the composite at S_0 = 4 shows the lowest resistance, its fracture strain is less than 50%. For all of the Ag−Cu fillers used in this work, the optimal S_0 is 3 and the solution viscosity is ∼1.5 Pa.s.

The corresponding cross-sectional SEM images of the composite films cast from varying S_0 are shown in Figure 8. The distribution of the flakes in the films is regulated by the competition between the sedimentation velocity and the solvent evaporation rate. The layer thickness of the flake sediments at the bottom increases with S_0, because in the solution with a lower viscosity, a higher sedimentation velocity allows the flakes to travel a longer distance before the films are frozen upon drying. The flakes are more evenly dispersed in the film at S_0 = 2 and thus unable to effectively form conductive channels to enhance the conductivity. At S_0 = 4, the large amount of the flakes sedimented at the bottom are advantageous to the conductivity. However, the sediment

https://doi.org/10.1021/acsapm.2c00801
ACS Appl. Polym. Mater. 2022, 4, 6871−6879

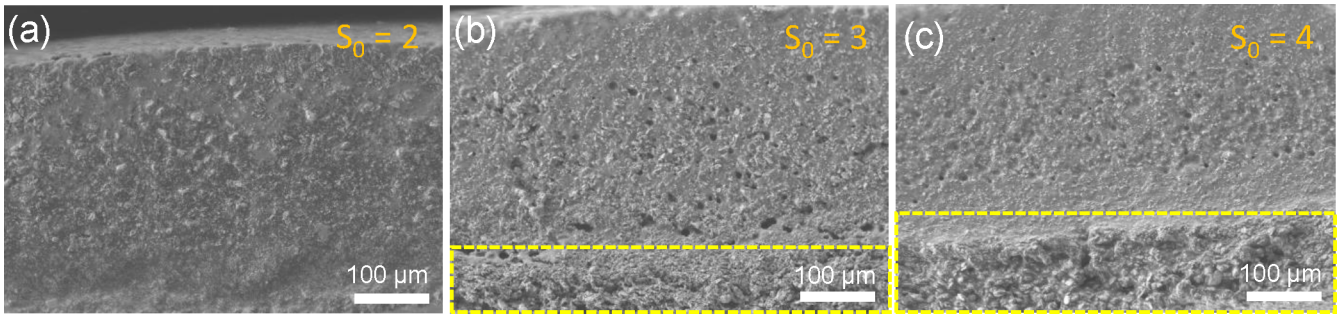

Figure 8. Cross-sectional SEM images of the composites cast from the solutions at (a) $S_0 = 2$, (b) $S_0 = 3$, and (c) $S_0 = 4$. The ~1 μm Ag−Cu flakes were used, and the weight ratio of F-rubber/Ag−Cu/[EMIM][Tf_2N] was fixed at 1:3:0.5.

where the flakes densely stack lacks a continuous rubber phase between the flakes to provide ductility. Cracks are thus readily created in the flake layer, leading to the low fracture strain of the composite. The viscosity (1.5 Pa s) of the solution at $S_0 = 3$ is optimal for the flakes and rubber to form the structure with a balanced performance in this system. The bottom flake-rich layer offers a high conductivity while containing a sufficient rubber phase to prevent cracking upon stretching. The top rubber-rich layer can hold the film and prevent the film from fracture, which makes a major contribution to the high stretchability of the composite. Note that the optimal viscosity of the solution may vary with systems and processes and requires it to be determined on a case-by-case basis.

3.5. Performance of Cross-linked F-rubber. An important design principle for stretchable electronics is to increase the durability of the materials. To achieve this purpose, F-rubber in the composites was cross-linked by the reagents of Luperox F and TAIC to enhance the elasticity and mechanical strength. The cross-linked samples are named with a *c*-F sign prefixed. Figure S8a shows the storage modulus G' of F-rubber without and with cross-linking treatment as functions of frequency. The G' of F-rubber after cross-linking is about 2 times higher than that without cross-linking. The G's of the cross-linked F-rubber in the presence of the ILs are shown in Figure S8b, where I_0's for [EMIM][Tf_2N], [EMIM][TfO], and [EMPY][Tf_2N] are 0.5, 0.1, and 0.2, respectively, which are the optimized ratios for each IL. A decrease in G' can be seen as the ILs are incorporated, evidencing the ILs as plasticizers to mobilize chain segments and soften F-rubber.

The resistance vs strain curves of the cross-linked composites with 15−20 μm Ag−Cu flakes at a weight ratio of F-rubber/Ag−Cu fixed at 1:1.5 are shown in Figure 9. Although the 15−20 μm flakes cause a low fracture strain of the composites, they give the lowest resistance among the fillers used in this work (Figure 5) and can reach the same conductivity level as that of the 3−5 μm flakes at half of the amount. The composites with ILs show a slower increase in resistance with strain and a higher fracture strain than that without IL (*c*-F-rubber) does, among which *c*-F-[EMPY][Tf_2N] at $I_0 = 0.2$ outperforms the others, with a fracture strain up to 340%. The cross-sectional SEM images of the cross-linked composite films are shown in Figure S9, where the flake-rich layers are sedimented at the bottom covered by the rubber-rich layers on the top. The stress−strain curves of the cross-linked composites are shown in Figure S10 and the mechanical properties are listed in Table S3, which are consistent with the effects of the ILs on the stretchability of the composites revealed in Figure 9.

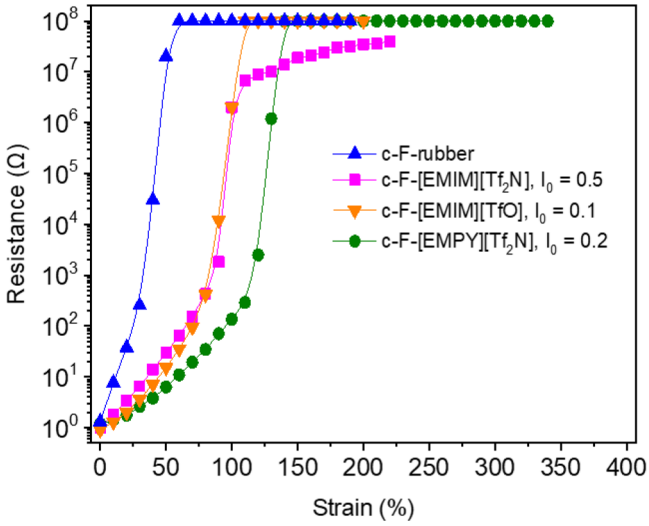

Figure 9. Resistance vs strain curves of the cross-linked composites with the ILs at the optimized I_0. The 15−20 μm Ag−Cu flakes were used, and the weight ratio of F-rubber/Ag−Cu was fixed at 1:1.5.

To examine the durability of the cross-linked composites, the cyclic stretch-release tests up to 100 cycles were conducted, and the data at 75% strain are shown in Figure 10. Both *c*-F-rubber and *c*-F-[EMPY][Tf_2N] (moderate miscibility) are able to endure 100 stretching cycles. The resistance of *c*-F-[EMPY][Tf_2N] slowly increases with the number of cycles, ~10^3 Ω at 40 cycles and below 10^6 Ω at 100 cycles, apparently more stable than that of *c*-F-rubber, which increases to nearly 10^8 Ω (the upper limit of the instrument) at 60 cycles. *c*-F-[EMIM][TfO] (low miscibility) breaks at 90 cycles, and surprisingly, *c*-F-[EMIM][Tf_2N] (high miscibility) almost loses conductivity immediately upon cyclic stretching and breaks at 60 cycles. The *c*-F-[EMPY][Tf_2N] film was utilized to serve as the conductive and flexible conductors in a circuit to light up a bulb, as shown in Figure S11. The bulb maintained high illumination when the film was repeatedly bent, folded, 360° twisted, and cyclic stretched at 125% strain.

Lastly, the explanation for the inferior performance of the *c*-F-[EMIM][Tf_2N] composite is proposed. The highly miscible nature of [EMIM][Tf_2N] with F-rubber is favorable for the conductive elastomers. However, the interactions between ILs and Ag−Cu fillers may be another factor that affects the performance of the conductive elastomers, which should also be considered. To clarify this point, Cu particles were placed in pure [EMIM][Tf_2N], and the sample was heated to 160 °C for 4.5 h. As shown in Figure S12, the sample turned dark green in

https://doi.org/10.1021/acsapm.2c00801
ACS Appl. Polym. Mater. 2022, 4, 6871−6879

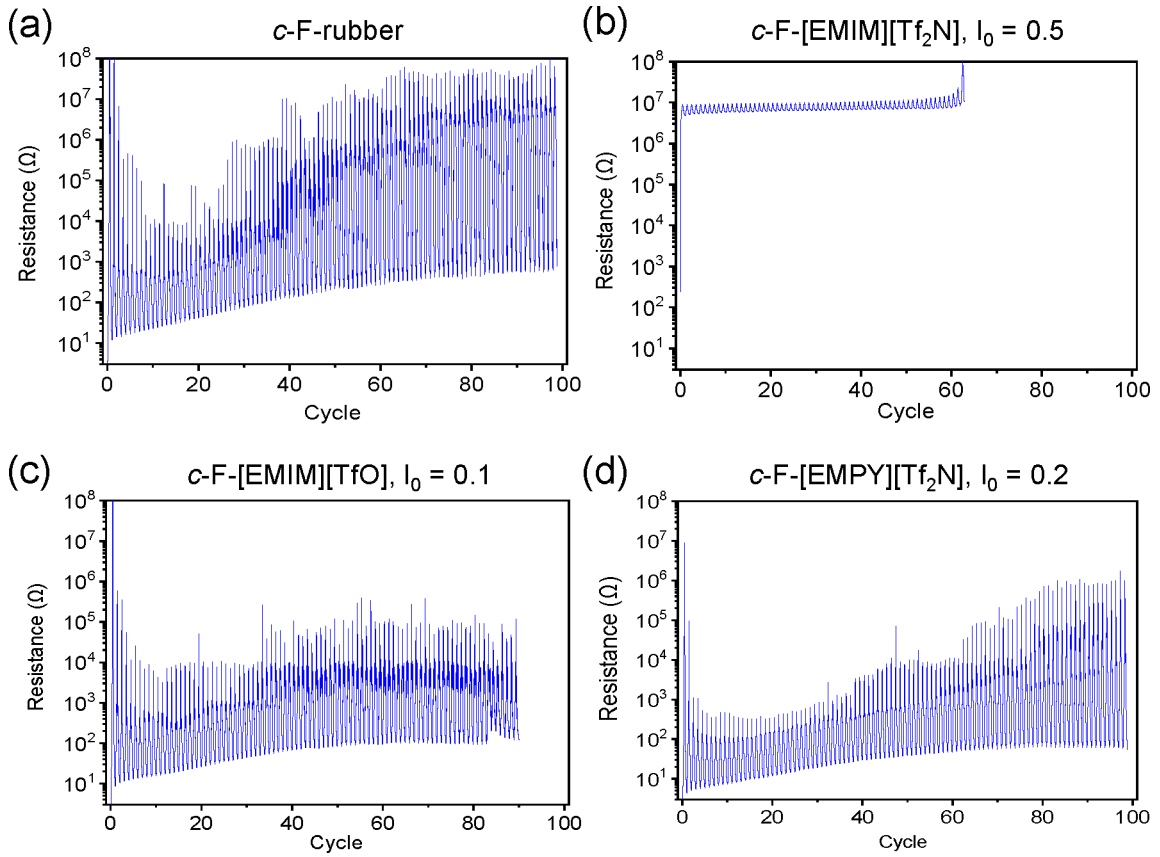

Figure 10. Cyclic stretch-release tests at 75% strain for the cross-linked composites with the ILs at the optimized I_0. (a) *c*-F-rubber, (b) *c*-F-[EMIM][Tf_2N], (c) *c*-F-[EMIM][TfO], and (d) *c*-F-[EMPY][Tf_2N]. The 15−20 μm Ag−Cu flakes were used, and the weight ratio of F-rubber/Ag−Cu was fixed at 1:1.5.

color, and F, Cu, S, and O elements were detected in the solid products by EDS. This change does not occur for the other two ILs. In other words, the Cu fillers tend to chemically react with [EMIM][Tf_2N], especially after the high-temperature treatment during the cross-linking process. Such a reaction causes two effects. First, [EMIM][Tf_2N] may be adsorbed onto Ag−Cu flakes due to the strong interaction, which explains why the composites require a high amount of [EMIM][Tf_2N] (I_0 > 0.4) to achieve high stretchability. Second, the oxide products on the flake surface may lower the conductivity, and the change in chemical structure of the IL after reaction may be responsible for the lower stretchability of the composites.

4. CONCLUSIONS

In this work, we studied the effects of the miscibility between the ionic liquids and fluorine rubber, the size and shape of the conductive fillers, and the viscosity of the casting solutions on the stretchability and conductivity of intrinsically stretchable conductive elastomers containing fluorine rubber, silver-coated copper fillers, and ionic liquids. Three ionic liquids of high, moderate, and low miscibility with fluorine rubber respectively were used, as evidenced by DSC and SAXS. The ionic liquids with high and moderate miscibility can significantly enhance the stretchability and conductivity of the composites, which manifests the key role of the miscibility between the additive and matrix in the composite conductive elastomers. Particular attention should be paid to the possible chemical reactions between ionic liquids and metal fillers that may cause negative effects on the composites. In addition, the distribution of the conductive fillers in the films was manipulated through varying the viscosity of the casting solutions to acquire the optimal structure with appropriate bottom filler-rich layer and top rubber-rich layer that impart conductivity and stretchability, respectively. The fluorine rubber was further cross-linked, which was demonstrated to improve the resilience and durability under cyclic stretching. The conductive elastomers developed in this work are potential for applications in flexible electronics and the fundamental findings can serve as the design principles for the exploitation of new stretchable conductors.

■ ASSOCIATED CONTENT

Supporting Information

The Supporting Information is available free of charge at https://pubs.acs.org/doi/10.1021/acsapm.2c00801.

Additional DSC, rheology, mechanical property, and EDS data; normalized resistance vs strain curves; SEM images and photographs of samples (PDF)

■ AUTHOR INFORMATION

Corresponding Author

Shih-Huang Tung − *Institute of Polymer Science and Engineering and Advanced Research Center for Green Materials Science and Technology, National Taiwan University, Taipei 10617, Taiwan;* orcid.org/0000-0002-6787-4955; Email: shtung@ntu.edu.tw

https://doi.org/10.1021/acsapm.2c00801
ACS Appl. Polym. Mater. 2022, 4, 6871−6879

Authors

Wen-Hsien Liu − *Institute of Polymer Science and Engineering, National Taiwan University, Taipei 10617, Taiwan*

I-Hung Huang − *Institute of Polymer Science and Engineering, National Taiwan University, Taipei 10617, Taiwan*

Yi-Ting Wu − *Institute of Polymer Science and Engineering, National Taiwan University, Taipei 10617, Taiwan*

Dai-Hua Jiang − *Institute of Polymer Science and Engineering, National Taiwan University, Taipei 10617, Taiwan*

Wei-Yang Ma − *Institute of Nuclear Energy Research, Atomic Energy Council, Executive Yuan, Taoyuan 32546, Taiwan*

Ying-Chih Liao − *Department of Chemical Engineering and Advanced Research Center for Green Materials Science and Technology, National Taiwan University, Taipei 10617, Taiwan;* orcid.org/0000-0001-9496-4190

Complete contact information is available at: https://pubs.acs.org/10.1021/acsapm.2c00801

Author Contributions

[⊥]W.-H.L. and I.-H.H. contributed equally to this paper

Notes

The authors declare no competing financial interest.

■ ACKNOWLEDGMENTS

This work was financially supported in part by the "Advanced Research Center of Green Materials Science and Technology" from the Featured Area Research Center Program within the framework of the Higher Education Sprout Project and in part by S.-H.T.'s research fundings, which are granted by the Ministry of Education (111L9006 and 110L891502) and the National Science and Technology Council (NSTC 106-3111-Y-042A-094, 109-2221-E-002-182-MY3, and 111-2634-F-002-016) in Taiwan. The authors thank National Synchrotron Radiation Research Center, Taiwan, for facilitating the X-ray scattering experiments.

■ REFERENCES

(1) Park, M.; Park, J.; Jeong, U. Design of conductive composite elastomers for stretchable electronics. *Nano Today* **2014**, *9*, 244−260.

(2) Li, Z.; Zhu, M.; Shen, J.; Qiu, Q.; Yu, J.; Ding, B. All-fiber structured electronic skin with high elasticity and breathability. *Adv. Funct. Mater.* **2020**, *30*, 1908411.

(3) Wang, L.; Jackman, J. A.; Tan, E.-L.; Park, J. H.; Potroz, M. G.; Hwang, E. T.; Cho, N.-J. High-performance, flexible electronic skin sensor incorporating natural microcapsule actuators. *Nano Energy* **2017**, *36*, 38−45.

(4) Wu, R.; Ma, L.; Patil, A.; Hou, C.; Zhu, S.; Fan, X.; Lin, H.; Yu, W.; Guo, W.; Liu, X. Y. All-textile electronic skin enabled by highly elastic spacer fabric and conductive fibers. *ACS Appl. Mater. Interfaces* **2019**, *11*, 33336−33346.

(5) Yang, Y.; Zhao, G.; Cheng, X.; Deng, H.; Fu, Q. Stretchable and Healable Conductive Elastomer Based on PEDOT: PSS/Natural Rubber for Self-Powered Temperature and Strain Sensing. *ACS Appl. Mater. Interfaces* **2021**, *13*, 14599−14611.

(6) Choi, S.; Han, S. I.; Kim, D.; Hyeon, T.; Kim, D.-H. High-performance stretchable conductive nanocomposites: materials, processes, and device applications. *Chem. Soc. Rev.* **2019**, *48*, 1566−1595.

(7) Sekitani, T.; Nakajima, H.; Maeda, H.; Fukushima, T.; Aida, T.; Hata, K.; Someya, T. Stretchable active-matrix organic light-emitting diode display using printable elastic conductors. *Nat. Mater.* **2009**, *8*, 494−499.

(8) Yi, F.; Wang, X.; Niu, S.; Li, S.; Yin, Y.; Dai, K.; Zhang, G.; Lin, L.; Wen, Z.; Guo, H.; Wang, J.; Yeh, M.-H.; Zi, Y.; Liao, Q.; You, Z.; Zhang, Y.; Wang, Z. L. A highly shape-adaptive, stretchable design based on conductive liquid for energy harvesting and self-powered biomechanical monitoring. *Sci. Adv.* **2016**, *2*, e1501624.

(9) Noh, J.-S. Conductive elastomers for stretchable electronics, sensors and energy harvesters. *Polymers* **2016**, *8*, 123.

(10) Jeong, C. K.; Lee, J.; Han, S.; Ryu, J.; Hwang, G.-T.; Park, D. Y.; Park, J. H.; Lee, S. S.; Byun, M.; Ko, S. H.; Lee, K. J. A hyper-stretchable elastic-composite energy harvester. *Adv. Mater.* **2015**, *27*, 2866−2875.

(11) Sun, H.; Han, Z.; Willenbacher, N. Ultrastretchable conductive elastomers with a low percolation threshold for printed soft electronics. *ACS Appl. Mater. Interfaces* **2019**, *11*, 38092−38102.

(12) Matsuhisa, N.; Kaltenbrunner, M.; Yokota, T.; Jinno, H.; Kuribara, K.; Sekitani, T.; Someya, T. Printable elastic conductors with a high conductivity for electronic textile applications. *Nat. Commun.* **2015**, *6*, 1−11.

(13) Kim, D. C.; Shim, H. J.; Lee, W.; Koo, J. H.; Kim, D. H. Material-Based Approaches for the Fabrication of Stretchable Electronics. *Adv. Mater.* **2020**, *32*, 29.

(14) Sim, K.; Rao, Z. Y.; Ershad, F.; Yu, C. J. Rubbery Electronics Fully Made of Stretchable Elastomeric Electronic Materials. *Adv. Mater.* **2020**, *32*, 1902417.

(15) Song, P.; Song, J.; Zhang, Y. Stretchable conductor based on carbon nanotube/carbon black silicone rubber nanocomposites with highly mechanical, electrical properties and strain sensitivity. *Composites, Part B* **2020**, *191*, 107979.

(16) Bokobza, L. Enhanced electrical and mechanical properties of multiwall carbon nanotube rubber composites. *Polym. Adv. Technol.* **2012**, *23*, 1543−1549.

(17) Sui, G.; Zhong, W.; Yang, X.; Zhao, S. Processing and material characteristics of a carbon-nanotube-reinforced natural rubber. *Macromol. Mater. Eng.* **2007**, *292*, 1020−1026.

(18) Kim, Y. A.; Hayashi, T.; Endo, M.; Gotoh, Y.; Wada, N.; Seiyama, J. Fabrication of aligned carbon nanotube-filled rubber composite. *Scr. Mater.* **2006**, *54*, 31−35.

(19) Noriman, N. Z.; Ismail, H. Properties of styrene butadiene rubber (SBR)/recycled acrylonitrile butadiene rubber (NBRr) blends: The effects of carbon black/silica (CB/Sil) hybrid filler and silane coupling agent, Si69. *J. Appl. Polym. Sci.* **2012**, *124*, 19−27.

(20) Wu, Y. P.; Zhao, W.; Zhang, L. Q. Improvement of Flex-Fatigue Life of Carbon-Black-Filled Styrene-Butadiene Rubber by Addition of Nanodispersed Clay. *Macromol. Mater. Eng.* **2006**, *291*, 944−949.

(21) Dong, W.; Li, W.; Long, G.; Tao, Z.; Li, J.; Wang, K. Electrical resistivity and mechanical properties of cementitious composite incorporating conductive rubber fibres. *Smart Mater. Struct.* **2019**, *28*, 085013.

(22) Alla, R. K.; Swamy, K. R.; Vyas, R.; Konakanchi, A.; Guduri, V.; Gadde, P. Influence of Silver nanoparticles incorporation on flexural strength of heat-cure acrylic denture base resin materials. *Annu. Res. Rev. Biol.* **2017**, *17*, 1−8.

(23) Ata, S.; Mizuno, T.; Nishizawa, A.; Subramaniam, C.; Futaba, D. N.; Hata, K. Influence of matching solubility parameter of polymer matrix and CNT on electrical conductivity of CNT/rubber composite. *Sci. Rep.* **2014**, *4*, 7232.

(24) Kotal, M.; Banerjee, S. S.; Bhowmick, A. K. Functionalized graphene with polymer as unique strategy in tailoring the properties of bromobutyl rubber nanocomposites. *Polymer* **2016**, *82*, 121−132.

(25) Li, H.; Yang, L.; Weng, G.; Xing, W.; Wu, J.; Huang, G. Toughening rubbers with a hybrid filler network of graphene and carbon nanotubes. *J. Mater. Chem. A* **2015**, *3*, 22385−22392.

(26) Subramaniam, K.; Das, A.; Heinrich, G. Development of conducting polychloroprene rubber using imidazolium based ionic liquid modified multi-walled carbon nanotubes. *Compos. Sci. Technol.* **2011**, *71*, 1441−1449.

(27) Ge, Q.; Liu, H. Z. Tunable amine-functionalized silsesquioxane-based hybrid networks for efficient removal of heavy metal ions and selective adsorption of anionic dyes. *Chem. Eng. J.* **2022**, *428*, 131370.

(28) Hussain, M.; Yasin, S.; Adnan Akram, M.; Xu, H.; Song, Y.; Zheng, Q. Influence of ionic liquids on structure and rheological

behaviors of silica-filled butadiene rubber. *Ind. Eng. Chem. Res.* **2019**, *58*, 18205−18212.
(29) Le, H.H.; Das, A.; Basak, S.; Tahir, M.; Wießner, S.; Fischer, D.; Reuter, U.; Stockelhuber, K.W.; Bhowmick, A.K.; Do, Q.K.; Heinrich, G.; Radusch, H.-J. Effect of different ionic liquids on the dispersion and phase selective wetting of carbon nanotubes in rubber blends. *Polymer* **2016**, *105*, 284−297.
(30) Lei, Y.; Tang, Z.; Zhu, L.; Guo, B.; Jia, D. Functional thiol ionic liquids as novel interfacial modifiers in SBR/HNTs composites. *Polymer* **2011**, *52*, 1337−1344.
(31) Yang, Q.; Zhang, Z.; Sun, X.-G.; Hu, Y.-S.; Xing, H.; Dai, S. Ionic liquids and derived materials for lithium and sodium batteries. *Chem. Soc. Rev.* **2018**, *47*, 2020−2064.
(32) Keskin, S.; Kayrak-Talay, D.; Akman, U.; Hortaçsu, Ö. A review of ionic liquids towards supercritical fluid applications. *J. Supercrit. Fluids* **2007**, *43*, 150−180.
(33) Forsyth, S. A.; Pringle, J. M.; MacFarlane, D. R. Ionic liquids—an overview. *Aust. J. Chem.* **2004**, *57*, 113−119.
(34) Shamsuri, A. A.; Daik, R.; Md. Jamil, S. N. A. A Succinct Review on the PVDF/Imidazolium-Based Ionic Liquid Blends and Composites: Preparations, Properties, and Applications. *Processes* **2021**, *9*, 761.
(35) Correia, D. M.; Fernandes, L. C.; Martins, P. M.; Garcia-Astrain, C.; Costa, C. M.; Reguera, J.; Lanceros-Mendez, S. Ionic Liquid-Polymer Composites: A New Platform for Multifunctional Applications. *Adv. Funct. Mater.* **2020**, *30*, 1909736.
(36) Scott, M. P.; Rahman, M.; Brazel, C. S. Application of ionic liquids as low-volatility plasticizers for PMMA. *Eur. Polym. J.* **2003**, *39*, 1947−1953.
(37) Wang, Y.; Zhu, C. X.; Pfattner, R.; Yan, H. P.; Jin, L. H.; Chen, S. C.; Molina-Lopez, F.; Lissel, F.; Liu, J.; Rabiah, N. I.; Chen, Z.; Chung, J. W.; Linder, C.; Toney, M. F.; Murmann, B.; Bao, Z. A highly stretchable, transparent, and conductive polymer. *Sci. Adv.* **2017**, *3*, 10.
(38) Teo, M. Y.; Kim, N.; Kee, S.; Kim, B. S.; Kim, G.; Hong, S.; Jung, S.; Lee, K. Highly Stretchable and Highly Conductive PEDOT:PSS/Ionic Liquid Composite Transparent Electrodes for Solution-Processed Stretchable Electronics. *ACS Appl. Mater. Interfaces* **2017**, *9*, 819−826.
(39) de Izarra, A.; Park, S.; Lee, J.; Lansac, Y.; Jang, Y. H. Ionic Liquid Designed for PEDOT:PSS Conductivity Enhancement. *J. Am. Chem. Soc.* **2018**, *140*, 5375−5384.
(40) Lei, Z. Y.; Wu, P. Y. A highly transparent and ultra-stretchable conductor with stable conductivity during large deformation. *Nat. Commun.* **2019**, *10*, 9.
(41) Guan, J.; Xing, C.; Wang, Y.; Li, Y.; Li, J. Poly (vinylidene fluoride) dielectric composites with both ionic nanoclusters and well dispersed graphene oxide. *Compos. Sci. Technol.* **2017**, *138*, 98−105.
(42) Fritzsche, J.; Lorenz, H.; Klueppel, M. CNT Based Elastomer-Hybrid-Nanocomposites with Promising Mechanical and Electrical Properties. *Macromol. Mater. Eng.* **2009**, *294*, 551−560.
(43) Chun, K. Y.; Oh, Y.; Rho, J.; Ahn, J. H.; Kim, Y. J.; Choi, H. R.; Baik, S. Highly conductive, printable and stretchable composite films of carbon nanotubes and silver. *Nat. Nanotechnol.* **2010**, *5*, 853−857.
(44) Abraham, J.; P., M. A.; Kailas, L.; Kalarikkal, N.; George, S. C.; Thomas, S. Developing highly conducting and mechanically durable styrene butadiene rubber composites with tailored microstructural properties by a green approach using ionic liquid modified MWCNTs. *RSC Adv.* **2016**, *6*, 32493−32504.
(45) Wang, J.; Chu, H.; Li, Y. Why single-walled carbon nanotubes can be dispersed in imidazolium-based ionic liquids. *ACS Nano* **2008**, *2*, 2540−2546.
(46) Yoo, S. J.; Li, L. J.; Zeng, C. C.; Little, R. D. Polymeric ionic liquid and carbon black composite as a reusable supporting electrolyte: Modification of the electrode surface. *Angew. Chem., Int. Ed. Engl.* **2015**, *127*, 3815−3818.
(47) Guldi, D. M.; Martín, N. Fullerene architectures made to order; biomimetic motifs—design and features. *J. Mater. Chem. A* **2002**, *12*, 1978−1992.
(48) Lueckmann, M.; Schuster, R. H.; Giese, U. Customized Performance Modification of Special Rubbers Using Ionic Liquids. *KGK-Kautsch. Gummi Kunstst.* **2016**, *69*, 38−45.
(49) Varol, T.; Guler, O.; Akcay, S. B.; Aksa, H. C. The effect of silver coated copper particle content on the properties of novel Cu-Ag alloys prepared by hot pressing method. *Powder Technol.* **2021**, *384*, 236−246.
(50) Song, J. Z.; Li, J. H.; Xu, J. Y.; Zeng, H. B. Superstable Transparent Conductive Cu@Cu4Ni Nanowire Elastomer Composites against Oxidation, Bending, Stretching, and Twisting for Flexible and Stretchable Optoelectronics. *Nano Lett.* **2014**, *14*, 6298−6305.
(51) Choi, S.; Han, S. I.; Jung, D.; Hwang, H. J.; Lim, C.; Bae, S.; Park, O. K.; Tschabrunn, C. M.; Lee, M.; Bae, S. Y.; Yu, J. W.; Ryu, J. H.; Lee, S. W.; Park, K.; Kang, P. M.; Lee, W. B.; Nezafat, R.; Hyeon, T.; Kim, D. H. Highly conductive, stretchable and biocompatible Ag-Au core-sheath nanowire composite for wearable and implantable bioelectronics. *Nat. Nanotechnol.* **2018**, *13*, 1048−1056.
(52) Seurer, B.; Coughlin, E. B. Fluoroelastomer Copolymers Incorporating Polyhedral Oligomeric Silsesquioxane. *Macromol. Chem. Phys.* **2008**, *209*, 2040−2048.
(53) Drobny, J. G. Fluoroelastomers. In *Introduction to Fluoropolymers*; Ebnesajjad, S., Ed.; Elsevier, 2013; pp 149−230.
(54) Liu, C. H.; Tseng, W. H.; Cheng, C. Y.; Wu, C. I.; Chou, P. T.; Tung, S. H. Effects of Amorphous Poly(3-hexylthiophene) on Active-Layer Structure and Solar Cells Performance. *J. Polym. Sci. Pt. B-Polym. Phys.* **2016**, *54*, 975−985.
(55) Chiang, Y. C.; Shih, C. C.; Tung, S. H.; Chen, W. C. Blends of polythiophene nanowire/fluorine rubber with multiscale phase separation suitable for stretchable semiconductors. *Polymer* **2018**, *155*, 146−151.

https://doi.org/10.1021/acsapm.2c00801
ACS Appl. Polym. Mater. 2022, 4, 6871−6879